encit 2020

ABCM
Associação Brasileira de Engenharia e Ciências Mecânicas

18th Brazilian Congress of Thermal Sciences and Engineering
November 16–20, 2020 (Online)

ENC-2020-0504
HEAT TRANSFER ENHANCEMENT STUDY IN MICRO SCALE USING A CO-FLOW DEVICE

V. C. Teixeira
A. G. B. da Cruz
Faculdade de Engenharia Mecânica/ITEC, Universidade Federal do Pará, Brazil
victor.c.teixeira@gmail.com
aguicruz@ufpa.br

G. M. Guerra
Departamento de Engenharia Mecânica/TEM, Universidade Federal Fluminense, Brazil
gguerra@id.uff.br
F. P. Duda
Programa de Engenharia Mecânica, COPPE/UFRJ, Rio de Janeiro, Brazil
duda@mecanica.coppe.ufrj.br

Abstract. *In this paper, we analyze the convective heat transfer enhancement in a cilyndrical microchannel using a co-flow device to periodically produce spherical immiscible droplets in a continuous liquid flow. We use a phase-field model consisting of the Navier-Stokes/Cahn-Hilliard equations coupled with the energy equation. Based on the local and average Nusselt number and the temperature field distribution, we discuss the heat exchange increase with the spherical droplet-laden flow, compared with the case of single-phase flow. The results suggests the existence of a optimal flow ratio between the immiscible phases giving the highest heat exchange within the microchannel.*

Keywords: *heat transfer, microchannel, droplets, phase-field.*

1. INTRODUCTION

Two-phase flows of immiscible liquids appear in the context of several applications. For instance, microdroplets have the capability of transport small volume ranging from microliters to milliliters and can be used as microreactors performing multiples reactions through the conditions modification within each droplet (Song *et al.* (2003)). In the studies by Fischer *et al.* (2010), flows involving droplets and slugs have the potential of enhancing heat transfer in microfluidic devices by inducing recirculation zones in the carrier fluid. Khater *et al.* (2019) showed that the high ratio of surface area to volume provided by the droplets guarantees a rapid response in the temperature change and that the dynamics of the droplets are influenced by the temperature. That is, the physical properties of the droplets and the phase carrier, such as density, viscosity and interfacial tension between two immiscible phases are temperature dependent. Controlling the stability of droplet transport in microchannels at high temperatures is still a challenge. In the work by Khater *et al.* (2019) this problem can be overcome by adding a surfactant in the transport phase. Understanding the thermal behavior of droplets being transported in a microchannel is crucial for applications involving, for example, biomaterials (Khater *et al.* (2020)), cell encapsulation, and bacteria in dispersed droplets (Ning *et al.* (2018)), and enzyme engineering based on droplets (Longwell *et al.* (2017)). In the majority of those works, the heat transfer provoked by droplets within microfluidic is what provides most of the aplications, either by the precise control, large enhancement or by periodicity in temperature change.

The main characteristic of two-phase immiscible flows, is the presence of an interface separating the two phases. Specifically in two immiscible liquid phases, where there is a high degree of topological change (for example, coalescence or droplet breakage), tracking the interface can be quite challenging (Lovrić *et al.* (2019)). Standard strategies for emulating interface tracking include using the VOF method (volume of fluid) Hirt and Nichols (1981); Wang *et al.* (2012); Bordbar *et al.* (2020), level-set Bellotti and Theillard (2019); Gibou *et al.* (2018); Theillard *et al.* (2019)), difuse interface methods Gurtin *et al.* (1996), front-tracking Agnese and Nürnberg (2019); Tryggvason *et al.* (2001), where each has advantages and disadvantages in describing the interface. Difuse interface (or phase field) methods have become an alternative for dealing with problems involving complex topology changes and represent the evolving interface (see, for example, Lovrić *et al.* (2019)). All these treatments consider the interface as a discontinuity region or sharp interfaces, the phase field model consider that the different phases are separated by three-dimensional transition zone through which the

material properties (specific mass, viscosity, thermal conductivity, etc.) which characterizes the phases vary smoothly over a very small length. This is achieved by introducing an order parameter, or phase field variable, for a smooth transition of different physical quantities in the interface zone. Phase field modeling, therefore, allows the modeling of interfacial phenomena, without *a-priori* assumptions about the shape of the moving interface.

In this paper, we analyze the thermal behavior of dispersed droplets in the co-flowing within a cylindrical microchannel subjecting to a temperature change in a co-flowing. For that, we consider an axisymmetric two-phase flow model coupling the hydrodynamic Navier-Stokes equations with Cahn-Hilliard and energy equations for simulating the physics of droplets transport in the microchannel. This coupling of the flow and phase-field equations is given by an extra surface tension force term in the flow equations and a fluid-induced transport term in the Cahn–Hilliard equation. Further, we study the thermal convective enhancement of microchannel by the vortices in continuous phase between droplets due to the presence of liquid-liquid interfaces. We assume a standard simplified model by considering droplets formation in a co-flowing and heat transfer as a Graetz problem. Water is used as a continuous phase at different flow rate ratios with oil used as a dispersed droplets phase.

This paper is organized as follows. In section 2 we introduce the problem definition and the governing equations for the two-phase flow. Then, in section 3, we describe the numerical details to solve the physical problem using a finite element implementation in the COMSOL Multiphysics. In section 4 we present results and discussion on the enhancement of the convective heat transfer based on the local Nusselt number and temperature distribution for a train of droplets moving in the bulk liquid flow. We finish in section 5 with some concluding remarks.

2. PROBLEM DEFINITION, GOVERNING EQUATIONS

We consider the microchannel geometry investigated by Fischer *et al.* (2010). Figure 1 shows a schematic representation of the studied geometry. The physical problem consists of liquid droplets produced by a co-flow device, which has as advantage not dealing with the contact of the interface with the microchannel wall. The droplets are formed in a isothermal, continuous fluid flow section. The flow through the channel embodies a hydrodynamically completely developed laminar flow and a thermally developing region. For single fluid flows, this physical system follows the standard Graetz problem. A train of droplets is immersed in the isothermic region of the cylindrical channel represented by the entrance region in Fig. 1. As they move with the continuous fluid, the flow develops around the droplets deforming the interface between the droplet and their surrounding immiscible liquid. After the two-immiscible liquids flow field is developed in the isothermal region, the train of droplets enters into the thermally developing region of the microchannel, represented in Fig. 1 by the heated region. Granted the above assumptions, the fluid flow in the entire physical domain is described by

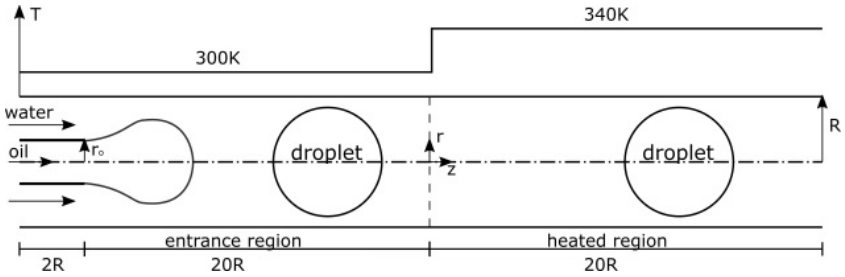

Figure 1. Physical problem scheme. The droplet trains are immersed into the isothermal bulk-fluid region.

the generalized Navier-Stokes/Cahn-Hilliard, continuity and energy equations

$$\left.\begin{aligned} \varrho(\varphi)\left(\frac{\partial \mathbf{v}}{\partial t}+\mathbf{v}\cdot\nabla\mathbf{v}\right) &= -\nabla p+\nabla\cdot\left(\mu(\varphi)(\nabla\mathbf{v}+(\nabla\mathbf{v})^{\top})\right)-\lambda(\Delta\varphi)\nabla\varphi,\\ \nabla\cdot\mathbf{v} &= 0,\\ \frac{\partial\varphi}{\partial t}+\nabla\cdot(\mathbf{v}\varphi) &= m\Delta\left(-\lambda\Delta\varphi+\frac{dg(\varphi)}{d\varphi}\right),\\ \varrho(\varphi)c(\varphi)\left(\frac{\partial T}{\partial t}+\mathbf{v}\cdot\nabla T\right) &= \nabla\cdot\left(k(\varphi)\nabla T\right). \end{aligned}\right\} \tag{1}$$

In $(1)_1$, p is the pressure field obtained to satisfy the incompressibility constraint $(1)_2$, $\varrho(\varphi)$ represents the specific mass density of the fluid, $\mu(\varphi)$ the viscosity of the fluid; the capillarity term $\lambda(\Delta\varphi)\nabla\varphi$ accounts for the surface tension force. We remark that the interfacial tension σ is calculated assuming a linear function with the temperature, where the Marangoni effect is included, i.e., $\sigma = f(T)$. The Cahn-Hilliard equation $(1)_3$ describes the evolution of the phase-field variable $\varphi(\mathbf{x}, t)$ (see Gurtin *et al.* (1996)), with a value of -1 for the dispersed phase and 1 for the continuous phase.

Here, Δ denotes the Laplacian operator, m represents the constitutive mobility parameter, given by

$$m = \chi\varepsilon^2, \tag{2}$$

with χ representing a mobility tuning parameter (see, e.g., Lim and Lam (2014); Bai *et al.* (2017)).

$$g(\varphi) = \frac{\lambda(\varphi^2-1)^2}{4\varepsilon^2} \tag{3}$$

represents a conventional double-well potential whose wells define the fluid phases, and leads to an interfacial layer within which the density φ suffers large variations (Gurtin *et al.* (1996)). The variable λ represents the mixing energy density, where we adopt the following conventional relation

$$\lambda = \frac{3\varepsilon\sigma}{2\sqrt{2}}. \tag{4}$$

It is interesting to note that the mixing energy density λ is related to the surface tension σ and the interfacial thickness ε. The mobility parameter m is We anticipate here that a very small value of χ may lead to numerical instabilities and extremely large values will not capture the interface evolving accurately.

In the energy equation $(1)_4$, $c(\varphi)$ and $k(\varphi)$ are the specific heat and thermal conductivity. It is interesting to note that the property fields in the physical domain are calculated as smooth functions of the phase variable φ, especially at the sharp limit interface (Bai *et al.* (2017)). Accordingly, we have used in our computation the following mass density and viscosity function given by

$$\varrho(\varphi) = \frac{(1-\varphi)}{2}\varrho_d + \frac{(1+\varphi)}{2}\varrho_c \tag{5}$$

and

$$\mu(\varphi) = \frac{(1-\varphi)}{2}\mu_d + \frac{(1+\varphi)}{2}\mu_c, \tag{6}$$

where ϱ_d and μ_d are the mass density and viscosity in the droplets (i.e., $\varphi = -1$) and ϱ_c and μ_c are the mass density and viscosity in continuous phase (i.e., $\varphi = 1$), respectively. The specific heat and thermal conductivity can be determined adopting the same method.

In our study case we have chosen a co-flow device to produce spherical droplets, the radius of the microchannel was set to $R = 500$ μm, with a length of $20R$ to capture the heat transfer behaviors in the heated entrance region and the inlet of the dispersed phase has a radius $r_0 = R/4$. The geometry of microchannel tube and the flow are axisymmetric (Fig. 1). Thus, we assume a symmetric boundary condition

$$\mathbf{v}\cdot\mathbf{n} = 0 \quad \text{and} \quad \mathbf{T}\mathbf{n} - (\mathbf{T}\mathbf{n}\cdot\mathbf{n})\mathbf{n} = \mathbf{0}, \tag{7}$$

where

$$\mathbf{T} = -p\mathbf{I} + 2\nu(\varphi)(\nabla\mathbf{v} + (\nabla\mathbf{v})^\top) + \lambda\nabla\varphi\otimes\nabla\varphi \tag{8}$$

is the stress tensor and $\mathbf{n}$ is the unit normal vector; the term $\lambda\nabla\varphi\otimes\nabla\varphi$ in the stress gives rise to normal stresses in the absence of flow and represents surface tension (Gurtin *et al.* (1996)). We set fix volumetric flow rate as boundary condition at the inlet for the dispersed and continuos phase. The mean velocity in the channel is fixed at $\upsilon = 10$ cm/s, which results in a flow Reynolds number of 50, i.e., a laminar flow regime. At the outlet boundary, we set the outflow boundary condition

$$\mathbf{T}\mathbf{n} = -p_0\mathbf{n} \tag{9}$$

with a fixed zero-pressure constraint $p_0 = 0$. For the Cahn-Hilliard equation $(1)_2$ we set the boundary condition

$$\mathbf{n}\cdot\mathrm{m}\nabla\left(-\lambda\Delta\varphi + \frac{dg(\varphi)}{d\varphi}\right) = 0 \quad \text{and} \quad \mathbf{n}\cdot\nabla\varphi = 0. \tag{10}$$

For the energy equation $(1)_4$, we set a temperature distribution as a step function along the microchannel wall, as shown in Fig. 1. In the isothermal inlet region, we assume the wall temperature as the bulk-fluid temperature $T = 300$ K, and in the heated region it is increased to 340 K. On the outlet boundary we set a zero-heat flux boundary condition

$$\mathbf{n}\cdot k(\varphi)\nabla T = 0. \tag{11}$$

3. NUMERICAL DETAILS, COMSOL

We have implemented and solved the afore-introduced model (1) in the finite-element software COMSOL using the Laminar Two-Phase Flow Module coupled to the Heat Transfer Module. The Chan-Hilliard equation $(1)_2$ is handled in COMSOL Multiphysics by adding an auxiliary variable to separate the fourth-order equation, thus resulting in two coupled second-order equations (see, e.g., Gomez and Hughes (2011), Song *et al.* (2003). We have adopted the following discretization and solver settings. A Lagrange linear shape functions for the pressure p and velocity $\mathbf{v}$ fields, with the Galerkin/least-squares stabilization, and linear shape functions for the others fields. Further, we used a implicit BDF time discretization with a free option, PARDISO direct solver with automatic damping, set up to recalculate the Jacobian matrix at each iteration.

4. RESULTS AND DISCUSSION

We begin our analysis by investigating the heat transfer enhancement in a microchannel for a train of spherical droplets of an immiscible liquid in the bulk fluid flow. The liquids we have used in this study are polyalphaolefine (PAO) as the dispersed phase and water as the continuous phase; see the physical properties in Table 1 of Fischer *et al.* (2010). In the present study, a co-flow device was used to periodically produce spherical droplets in a dripping regime. The process of droplet formation is divided in two stages, growing and detaching, as shown in Fig.2 at the time of 0.37s and 0.379s the droplet volume grows and when the interfacial tension can no longer hold a semi-spherical interface, it forms a neck and finally is detached from the inlet as shown in Fig. 2(see Wu *et al.* (2017)). The inlet of the carrying liquid, in our case, water, was set at a fixed volumetric flux, equivalent for a Reynolds number of 50, meaning that only the dispersed phase flux vary when changing the flow ratio

$$\alpha = \frac{Q_d}{Q_c}, \tag{12}$$

where Q_d and Q_c are the flux of the dispersed and continuous phase respectively. For the interfacial tension, we chose a linear function with the temperature, as adopted from Fischer *et al.* (2010) and given by

$$\sigma(T) = \sigma_0 + \sigma_T(T - 300) \tag{13}$$

where σ_0 is the interfacial tension at $300K$, equivalent to $38mNm^{-1}$ and the linear coefficient σ_T equal to $0,06mNm^{-1}K^{-1}$. In order to analyze the influence of the different flow ratios over the heat transfer, we have set our simulations for α ranges

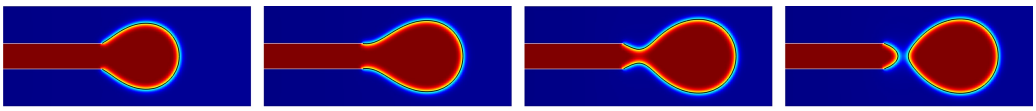

Figure 2. Droplet formation stages.

from 0.1 to 0.325, being the upper limit the maximum flow ratio where the droplets are produced periodically characterizing a dripping regime. In Figure 3 we can see in the heated region a periodic pattern of the droplets for some of different flow ratios. The heat transfer within the microchannel can be measured by the Nusselt number which is given by

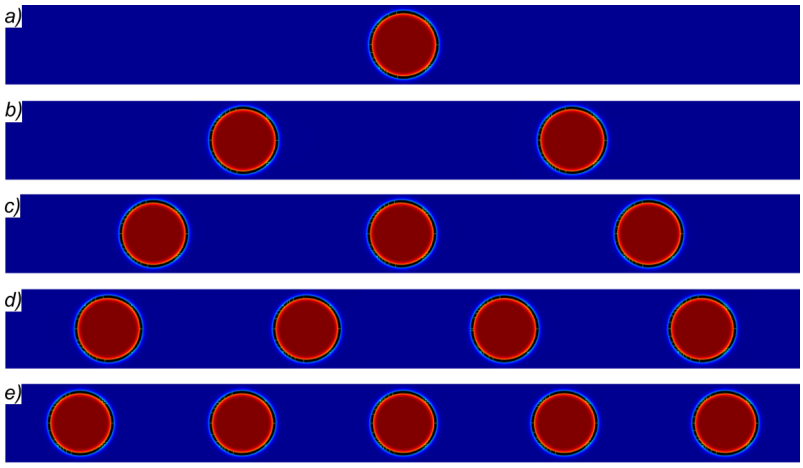

Figure 3. Two-phase flow simulations for (a) $\alpha = 0.1$, (b) $\alpha = 0.15$, (c) $\alpha = 0.2$, (d) $\alpha = 0.25$ and (e) $\alpha = 0.3$.

$$Nu = \frac{2R\left(\frac{\partial T}{\partial r}\right)_{r=R}}{K\left(T_b - T_{wall,z}\right)}, \tag{14}$$

where K is thermal conductivity. T_b is the average temperature over a cross section of the microchannel and is given by

$$T_b = \frac{\int_0^R \varrho c_p v_z T r dr}{\int_0^R \varrho c_p v_z r dr}, \tag{15}$$

where v_z is the z component of the velocity and $T_{wall,z}$ is the wall temperature. By this way we could calculate the local Nusselt number from the the simulation results. The Fig. 4 shows the results for the local Nusselt number and temperature distribution in the axial direction where a comparison between our result and the result by Fischer *et al.* (2010) is made as validation. It is interesting to note that in the presence of the train of droplets, the Nusselt number is significantly higher compared to the single liquid flow. This behavior is caused by the train of droplets being transported with a velocity greater than the bulk liquid mean velocity, in our particular case, approximately $14.6cm/s$. We observe the formation of

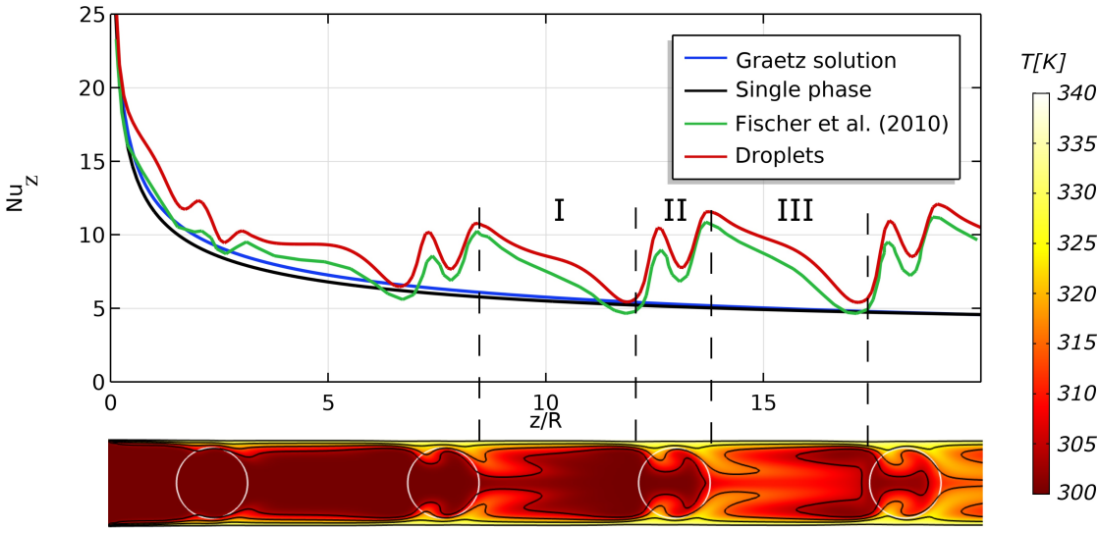

Figure 4. Local Nusselt number.

periodic patterns in the local Nusselt number profile represented in the graphic by the sections I, II, and III. Such periodic process provides a significant increase of the local Nusselt number until the end of the channel domain, $z/R = 20$, meaning a enhancement in the convection transport within the microchannel, as we can see in the Fig. 4 in sections I and II. Some of our results for the temperature field for the heated region with the length of 20R can be seen in Fig. 6 and it demonstrate the mixing capability caused by the droplets transport within the microchannel when compared to the single phase flow. The temperature distribution in the droplets and bulk-fluid also indicates that hotter liquid is being transported from the heated wall towards the center line of the channel where the liquid is colder, forming recirculation zones as can be seen in Fig. 5 by the streamlines for a reference moving frame for $\alpha = 0.2$. Thus, we find that the liquid in front of the droplets is hotter than the liquid in the rear, with a strong increase in the local Nusselt number. A similar process occurs in the droplets (see section II); within the droplets, the recirculation is more pronounced (Fig. 5). With a better

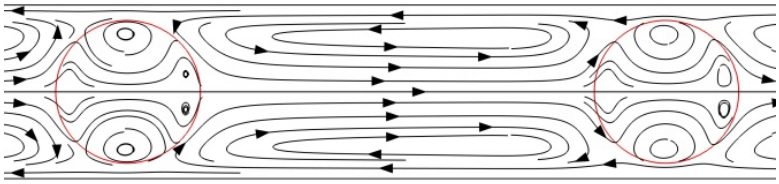

Figure 5. Recirculation zones in reference moving frame for the train of droplets.

look in Fig. 6 is also possible to verify that the temperature field becomes more dispersed as the flow ratio α increases up to a limit and as the flow ratio keeps rising we can see that the mixing capability decreases, pointing to the existence of a flow ratio that will correspond to a optimal mixing and consequentially to a optimal heat transfer by convection within the microchannel.

Through the number of vorticity, given by the relation

$$\omega = \frac{|\nabla \times \mathbf{v}|}{|\mathbf{D}|}, \tag{16}$$

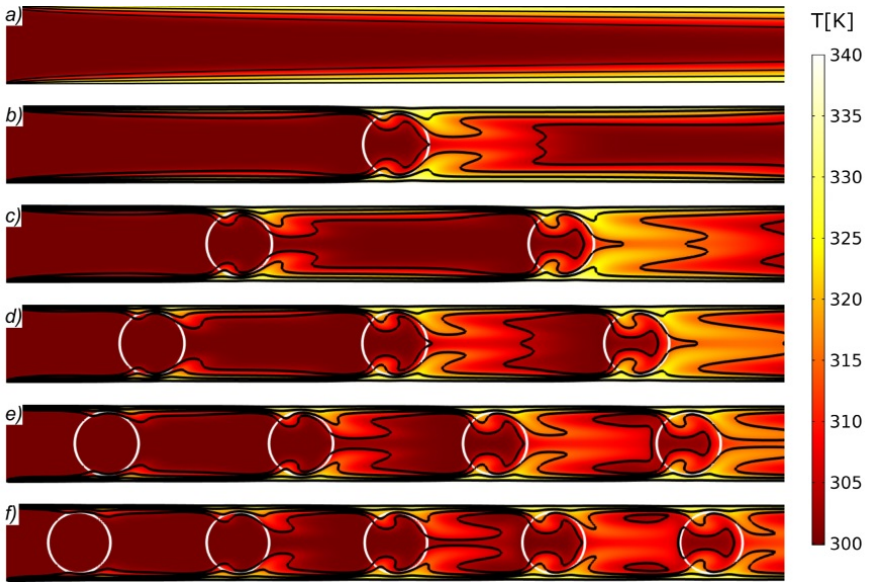

Figure 6. Temperature field for a (a) single phase flow and two phase flow for (b) $\alpha = 0.1$, (c) $\alpha = 0.15$, (d) $\alpha = 0.2$, (e) $\alpha = 0.25$ and (f) $\alpha = 0.3$.

we have a better understanding of the internal structure of the flow, where $\mathbf{D} = \frac{1}{2}\left(\nabla\mathbf{v} + \nabla\mathbf{v}^T\right)$ is the stretching rate tensor (see, e.g., Gross and Reusken (2011)). The vorticity number field for some different flow ratio scenarios in Fig. 7 give us the regions within the microchannel where rotation prevails over stretching rate and vice-versa, that is, the intensity and size of the recirculations shown in Fig. 5. Thus, we can confirm that the recirculation within each droplet is more intense than the recirculations in the bulk liquid. When increasing α more and smaller recirculation zones appears, but also more stretching prevalence zones, represented by the darker areas, which also suggests the existence of a optimal flow ratio that will produce more rotation over stretching and consequently more mixing. To compare the effect of many

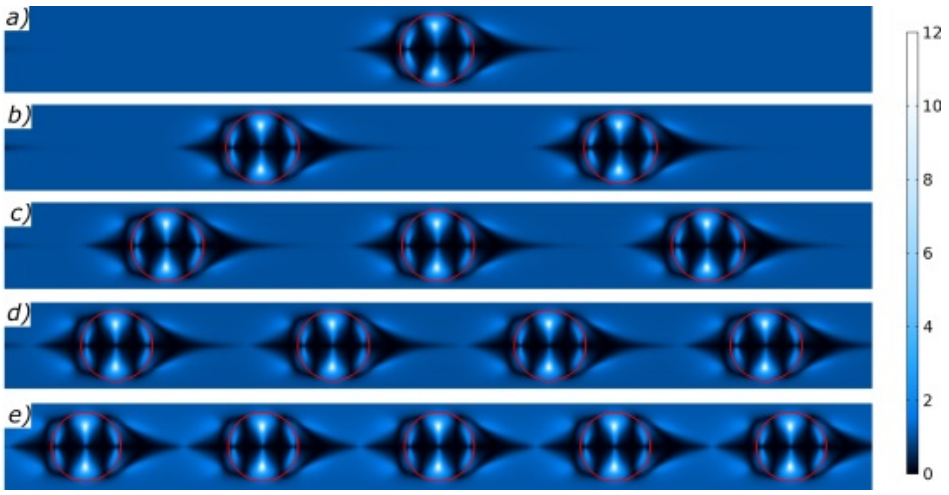

Figure 7. Vorticity number field for (a) $\alpha = 0.1$, (b) $\alpha = 0.15$, (c) $\alpha = 0.2$, (d) $\alpha = 0.25$ and (e) $\alpha = 0.3$.

different flow ratios more precisely over the heat transport and check the existence of a optimal flow ratio for our study case, we analyze the time and spatial average of the Nusselt number in the heated region. The results are shown in Fig. 8 and Fig. 9 as function of the flow ratio between both phases for the temporal averaged and spatial average Nusselt number respectively compared to the solution of aqueous single liquid flow. Those results suggest the existence of an optimal flow ratio related to maximum average Nusselt number between the flow ratios of 0.225 and 0.25, the loss of mixing capability is explained by the substitution of water for PAO with lower heat capacity and heat conductivity and also by the interruption of mixing due approximation of the droplets.

It is important to note that those results are predictions based on the phase field model using a specific droplet formation device, flow regime, microchannel geometry, and thermal properties. A validation of those predictions is needed through experimental studies.

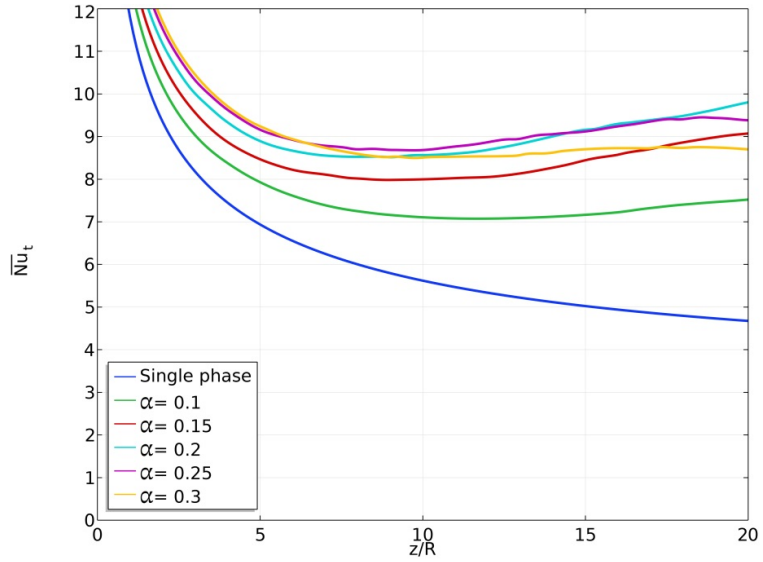

Figure 8. Nusselt number averaged over time for single phase flow and two phase flow for diferent flow ratios.

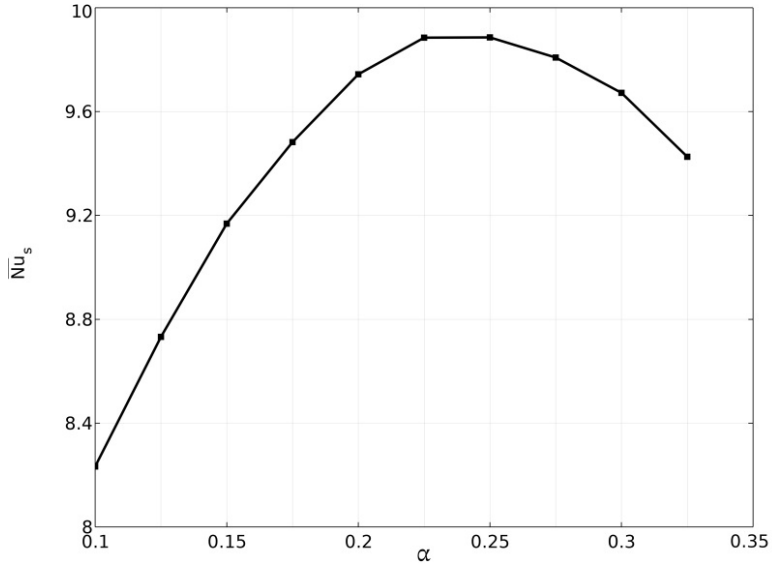

Figure 9. Average Nusselt number as function of flow ratio α.

5. CONCLUSIONS

This work dealt with the thermal transport of immiscible liquid-liquid flow through cylindrical microchannels. We have adopted a phase-field method for tracking the interface between the liquids. In the analysis, we have achieved similar results as presented by Fischer *et al.* (2010) for the local and averaged Nusselt numbers and temperature distribution. Simulation results showed a large enhancement in heat exchange, demonstrated by a pronounced increase in the local Nusselt number. We also predict the existence of a optimal flow ratio that provides the largest enhancement in the heat transfer.

6. ACKNOWLEDGEMENTS

The authors acknowledge the Coordenação de Aperfeiçoamento de Pessoal de Nível Superior–CAPES for support (Finance Code: 88881.200549/2018-01).

7. REFERENCES

Agnese, M. and Nürnberg, R., 2019. "Fitted front tracking methods for two-phase incompressible navier–stokes flow: Eulerian and ale finite element discretizations". *arXiv preprint arXiv:1910.14327*.

Bai, F., He, X., Yang, X., Zhou, R. and Wang, C., 2017. "Three dimensional phase-field investigation of droplet forma-

tion in microfluidic flow focusing devices with experimental validation". *International Journal of Multiphase Flow*, Vol. 93, pp. 130–141.

Bellotti, T. and Theillard, M., 2019. "A coupled level-set and reference map method for interface representation with applications to two-phase flows simulation". *Journal of Computational Physics*, Vol. 392, pp. 266–290.

Bordbar, A., Kamali, R. and Taassob, A., 2020. "Thermal performance analysis of slug flow in square microchannels". *Heat Transfer Engineering*, Vol. 41, No. 1, pp. 84–100.

Fischer, M., Juric, D. and Poulikakos, D., 2010. "Large convective heat transfer enhancement in microchannels with a train of coflowing immiscible or colloidal droplets". *Journal of Heat Transfer*, Vol. 132, No. 11, p. 112402.

Gibou, F., Fedkiw, R. and Osher, S., 2018. "A review of level-set methods and some recent applications". *Journal of Computational Physics*, Vol. 353, pp. 82–109.

Gomez, H. and Hughes, T.J., 2011. "Provably unconditionally stable, second-order time-accurate, mixed variational methods for phase-field models". *Journal of Computational Physics*, Vol. 230, No. 13, pp. 5310–5327.

Gross, S. and Reusken, A., 2011. *Numerical methods for two-phase incompressible flows*, Vol. 40. Springer Science & Business Media.

Gurtin, M.E., Polignone, D. and Vinals, J., 1996. "Two-phase binary fluids and immiscible fluids described by an order parameter". *Mathematical Models and Methods in Applied Sciences*, Vol. 6, No. 06, pp. 815–831.

Hirt, C.W. and Nichols, B.D., 1981. "Volume of fluid (vof) method for the dynamics of free boundaries". *Journal of computational physics*, Vol. 39, No. 1, pp. 201–225.

Khater, A., Abdelrehim, O., Mohammadi, M., Azarmanesh, M., Janmaleki, M., Salahandish, R., Mohamad, A. and Sanati-Nezhad, A., 2020. "Picoliter agar droplet breakup in microfluidics meets microbiology application: numerical and experimental approaches". *Lab on a Chip*.

Khater, A., Mohammadi, M., Mohamad, A. and Nezhad, A.S., 2019. "Dynamics of temperature-actuated droplets within microfluidics". *Scientific reports*, Vol. 9, No. 1, pp. 1–11.

Lim, C.Y. and Lam, Y.C., 2014. "Phase-field simulation of impingement and spreading of micro-sized droplet on heterogeneous surface". *Microfluidics and nanofluidics*, Vol. 17, No. 1, pp. 131–148.

Longwell, C.K., Labanieh, L. and Cochran, J.R., 2017. "High-throughput screening technologies for enzyme engineering". *Current opinion in biotechnology*, Vol. 48, pp. 196–202.

Lovrić, A., Dettmer, W.G. and Perić, D., 2019. "Low order finite element methods for the navier-stokes-cahn-hilliard equations". *arXiv preprint arXiv:1911.06718*.

Ning, R., Zhuang, Q. and Lin, J.M., 2018. "Biomaterial-based microfluidics for cell culture and analysis". In *Cell Analysis on Microfluidics*, Springer, pp. 181–224.

Song, H., Tice, J.D. and Ismagilov, R.F., 2003. "A microfluidic system for controlling reaction networks in time". *Angewandte Chemie International Edition*, Vol. 42, No. 7, pp. 768–772.

Theillard, M., Gibou, F. and Saintillan, D., 2019. "Sharp numerical simulation of incompressible two-phase flows". *Journal of Computational Physics*, Vol. 391, pp. 91–118.

Tryggvason, G., Bunner, B., Esmaeeli, A., Juric, D., Al-Rawahi, N., Tauber, W., Han, J., Nas, S. and Jan, Y.J., 2001. "A front-tracking method for the computations of multiphase flow". *Journal of computational physics*, Vol. 169, No. 2, pp. 708–759.

Wang, Z., Yang, J. and Stern, F., 2012. "A new volume-of-fluid method with a constructed distance function on general structured grids". *Journal of Computational Physics*, Vol. 231, No. 9, pp. 3703–3722.

Wu, L., Liu, X., Zhao, Y. and Chen, Y., 2017. "Role of local geometry on droplet formation in axisymmetric microfluidics". *Chemical Engineering Science*, Vol. 163, pp. 56–67.